Earth and Planetary Science Letters 554 (2021) 116697

Contents lists available at ScienceDirect

Earth and Planetary Science Letters

www.elsevier.com/locate/epsl

Mid-infrared spectroscopy of crystalline plagioclase feldspar samples with various Al,Si order and implications for remote sensing of Mercury and other terrestrial Solar System objects

Maximilian P. Reitze [a,*], Iris Weber [a], Andreas Morlok [a], Harald Hiesinger [a], Karin E. Bauch [a], Aleksandra N. Stojic [a], Jörn Helbert [b]

[a] Institut für Planetologie, Westfälische Wilhelms-Universität (WWU) Münster, 48149 Münster, Germany
[b] Deutsches Zentrum für Luft- und Raumfahrt (DLR), Rutherfordstr. 2, 12489 Berlin, Germany

ARTICLE INFO

Article history:
Received 9 September 2020
Received in revised form 19 November 2020
Accepted 22 November 2020
Available online 30 November 2020
Editor: W.B. McKinnon

Keywords:
plagioclase feldspar
Al,Si distribution
infrared spectroscopy
MERTIS
Mercury
space weathering

ABSTRACT

We analyzed plagioclase feldspar samples that were well-characterized in terms of chemical composition as well as degree of Al,Si order in mid-infrared reflection spectra between 7 µm and 14 µm (1429 cm^{-1} and 714 cm^{-1}). The chemical compositions were derived with an electron microprobe analyzer. To determine the degree of Al,Si order, powder X-ray diffraction methods were applied. For the interpretation of the infrared spectra, we used the wavelength of the Christiansen feature (CF) and the autocorrelation function for a specific wavelength region. The CF shifts from around 7.72 µm (1296 cm^{-1}) in Na-richest samples to 8.10 µm (1234 cm^{-1}) in the Ca-richest sample. Combining the CF position and the autocorrelation-derived value allowed to determine the degree of Al,Si order of the samples based on reflection spectra. The wavelength of the Transparency feature (TF) in the finest analyzed grain size fraction also depends on the chemical composition and the degree of Al,Si order. Our results are helpful for the interpretation of data returned by the MERTIS experiment onboard BepiColombo. The data help to distinguish between space weathering, shock effects, and ordering effects in plagioclase samples.

1. Introduction

1.1. Remote sensing of Mercury and the importance of analog measurements

Remote sensing is a common technique to explore planets, moons, and asteroids in the Solar System. The first spacecraft visiting Mercury was Mariner 10 in the 1970s, which mapped approximately half of the surface (Murray, 1975). The second mission to Mercury, MESSENGER (MErcury Surface, Space ENvironment, GEochemistry and Ranging), was in orbit around the planet between 2011 and 2015 (see Solomon et al., 2018, for a detailed description). In addition, in the time between these two missions, several Earth-based measurements of Mercury's surface were performed (e.g., Vilas et al., 1988; Sprague et al., 1995, 1997, 2009; Harmon et al., 2011). All these studies of Mercury gave new insights in the planet's structure but also left open questions. Concerning the surface mineralogy of Mercury, especially the feldspar composition, the overall picture is diverse. For example, the Gamma-Ray spectrometer (GRS) onboard the MESSENGER measured high Mg/Si and low Al/Si and Ca/Si contents that exclude an anorthite-rich feldspatic crust (Nittler et al., 2011). GRS detected relatively high abundances of sodium, which suggest that albite is a major mineral on the surface of Mercury (Evans et al., 2012). In contrast, Earth-based observations of Mercury's equatorial regions indicate a crust with a labradoritic composition at approximately 120° longitude as well as a region around 30° longitude with an anorthitic composition (Sprague et al., 1997). Recent chemical composition studies based on MESSENGER X-ray, gamma-ray, and neutron spectrometer data suggest a high content of albitic feldspar on the surface (Vander Kaaden et al., 2017).

To further investigate Mercury, the ESA/JAXA BepiColombo mission was launched to explore this innermost planet. Among other instruments, BepiColombo carries MERTIS (MErcury Radiometer and Thermal Infrared Spectrometer) that investigates Mercury's surface mineralogy in the wavelength region from 7 µm to 14 µm (TIS Spectrometer Channels, 1429 cm^{-1} and 714 cm^{-1}) (Hiesinger and Helbert, 2010; Hiesinger et al., 2020). The goals of MERTIS are the identification and mapping of the surface mineralogy as well as studying the surface temperatures and its thermal inertia (Hiesinger and Helbert, 2010; Hiesinger et al., 2020). In preparation

* Corresponding author.
E-mail address: maximilian.p-reitze@uni-muenster.de (M.P. Reitze).

https://doi.org/10.1016/j.epsl.2020.116697
0012-821X/

of the MERTIS experiment onboard BepiColombo (Hiesinger and Helbert, 2010; Hiesinger et al., 2020) and for potential other space missions equipped with thermal infrared spectrometers, we are building a high quality mid-infrared database of well-characterized samples (including, e.g., chemical composition and Raman spectra) (Weber et al., 2018; Morlok et al., 2019).

Recent analyses of planetary analog materials besides the feldspar studies concern the differences between basalt melts and impact-induced melts originating of basaltic material (Morlok et al., 2020), which showed, that these different melts show characteristic infrared spectra. Simulated micrometeorite bombardment on olivine and pyroxene revealed a decrease of reflectance and the production of fine-grained powder causing a Transparency feature (TF) in the mid-infrared spectra due to the simulated bombardment (Weber et al., 2020). Varatharajan et al. (2019) analyzed sulfides as analog material, that may be present on Mercury's surface, which has a mean sulfur abundance of around 4 wt% (Nittler et al., 2011). Synthetic rock glasses with Mercury surface composition were produced with X-ray spectrometer data provided by the MESSENGER mission to study mid-infrared spectral differences of these glasses and minerals with these particular compositions (Morlok et al., 2017).

For the identification of the mineralogical compositions of planetary surfaces, mid-infrared spectroscopy is particularly useful since silicate minerals in this wavelength range show characteristic absorption and reflectance bands due to vibrations of the Si and O framework (e.g., Pieters and Englert, 1993). For a correct interpretation of the spectra returned from space missions, detailed knowledge of the samples and factors that control the mineral samples' spectra are essential.

1.2. Plagioclases

Plagioclases are the solid solution between the sodium-rich endmember ($NaAlSi_3O_8$ denoted as Ab) on the one side and the calcium-rich endmember ($CaAl2Si_2O_8$ denoted as An) on the other side. In addition, the plagioclase solid solution can contain small proportions of $KAlSi_3O_8$ (denoted as Or). The crystal structure contains four non-equivalent tetrahedral sites T_10, T_1m, T_20, and T_2m, which are occupied by Si or Al ions (see Ribbe, 1983, for a detailed introduction).

The behavior in the mid-infrared spectral range of the sodium-rich endmember according to its state of order (low to high albite/analbite) was discussed in detail in Reitze et al. (2020) as part of the alkali feldspar system. Alkali feldspars are the solid solution between the endmembers Or and Ab (Ribbe, 1983). Reitze et al. (2020) successfully applied autocorrelation technique to the alklai feldspar spectra and found that the mid-infrared behavior of the albite series is strongly affected by the distribution of Al and Si in the different tetrahedral sites. In low albite, all Al-ions are located at the T_10 site, the probability to find an Al-ion on this site (t_10) is 1. In high albite/monalbite, the Al-ions are randomly distributed over all four tetrahedral sites, which results in a (hypothetical) probability to find an Al-ion in one of the sites of 0.25 (actually the T_10 site is always slightly preferred and t_10 is around 0.27 for highest disorder (Scambos et al., 1987)).

In this study, we focused on the mid-infrared spectra of plagioclases to analyze the degree of Al,Si order. Natural plagioclases as well as crystals formed synthetically by melting and crystallizing the appropriate oxides always have a remaining degree of order and are therefore topochemically triclinic (Kroll and Ribbe, 1980). The substitution of Na by Ca in the plagioclase solid solution must include a substitution of Si by Al to ensure charge balance. The An endmember needs a Si:Al ratio of 1:1 and Al-O-Al connections are unfavorable (Loewenstein, 1954). In contrast to the Al,Si distribution of the Ab endmember, the Al,Si distribution of the An endmember is always completely *ordered* in an alternating sense (Loewenstein, 1954). Therefore, the probability to find an Al-ion in one of the four tetrahedrons in the An crystals is always 0.25. Consequentially, a complete low-temperature solid solution between (low) albite and anorthite is impossible. In contrast to a complete low-temperature solid solution, diffusion of Na and Si as well as Ca and Al lead to the formation of three miscibility gaps. These are the peristerite gap ranging from An_2 to An_{25}, the Bøggild gap ranging from An_{38} to An_{62}, and the Huttenlocher gap ranging from An_{64} to An_{90}. The lamellae of the exsolution spacing is mostly submicroscopic, although, Huttenlocher exsolution is sometimes microscopically visible. However, exsolution should not be visible in mid-infrared spectra (Hecker et al., 2010). Rock cooling occurs often rapidly or at different cooling rates, thus metastable feldspar modifications in terms of Al,Si order and degree of exsolution can be preserved and be present on planetary surfaces.

Fundamental work on infrared absorption spectra of the feldspar system was done, for example, by Laves and Hafner (1956) and Hafner and Laves (1957), who showed that the degree of Al,Si order has an influence on the infrared absorption spectra of plagioclases. Lyon (1964) provided a spectral catalog with the wavelengths of peak positions for plagioclases with different chemical compositions. The An content of plagioclases could be determined independent from the degree of vitrification based on the wavelength of the Christiansen feature (CF) (Conel, 1970; Nash and Salisbury, 1991), which is a broad minimum in reflectance spectra or maximum in emission spectra.

In addition to the effects resulting of chemical composition or degree of order that influences the feldspars described above, feldspars on atmosphereless planetary bodies like Moon, Mercury or asteroids, are exposed to small and large impacts as well as radiation originating from the Sun and Galaxy, which is referred to as space weathering (e.g., Bennett et al., 2013, and references therein). These processes rework those surfaces and lead to changes of the minerals present on the surface. This is especially true for Mercury, because space weathering on its surface is much more intense due to its position in the Solar System compared to the Moon (Cintala, 1992). Space weathering processes have an influence on the form of the mid-infrared spectra of minerals and especially plagioclases (see e.g., Johnson et al., 2003; Moroz et al., 2014, for impact-induced shock and simulated micrometeorite bombardment, respectively). Ostertag (1983) investigated experimentally shocked (up to 45 GPa) feldspars to simulate larger impacts and showed that shock in their experimental setup does not affect the degree of Al,Si order not even during the formation of diaplectic glass. After the shock event, the samples were quenched to reduce the residual temperature caused by the impact. Nevertheless, the infrared transmission spectra of the feldspars changed significantly because of the formation of diaplectic glass. After heating of the shocked samples to temperatures between 800 °C and 1000 °C, Ostertag and Stöffler (1982) observed a rapid change of the Al,Si order.

1.3. Aim of this study

Therefore, the aim of this study is to investigate the plagioclase series in the mid-infrared with respect to both, the chemical composition and the ordering of Al and Si to provide a database, which allows the identification of feldspars with varying compositions and structural states. This information is crucial for a correct identification and characterization of feldspar minerals and a distinction of space weathering effects, such as large impacts and micrometeorite bombardment.

2. Samples and analyses

2.1. Characterization

Samples ID 126 and ID 127 are synthetic plagioclase crystals. They were synthesized from a melt with the specific composition of oxides and then crystallized at high pressures and temperatures. The Ab samples with different degree of order (IDs 164, 165, 166, 167) were produced by heating of a natural low albite (ID 125) from Cazadero (California) for different time intervals. For details of the synthesis process of these samples see Reitze et al. (2020). Samples ID 2 (unknown location in Scotland), 5 (unknown location), 6 (Södermanland, Sweden), 28 (Ihosy, Madagascar), 84 (Iveland, Norway), 168 (Saint-Raphaèl, Dep. Var, France), and 190 (Lake View, Oregon, USA) are untreated natural crystals.

Sample characterization of natural samples started with polarization microscopy to check for impurities within the sample. Afterwards, all samples were analyzed with the JEOL JXA-8530F Hyperprobe electron probe microanalyzer (EMPA) at Institut für Mineralogie (IfM) at the Westfälische Wilhelms-Universität Münster to determine their chemical compositions. To investigate the lattice parameters and degree of Al,Si order, powder X-ray diffraction patterns were obtained with an Phillips X'Pert powder diffractometer, at IfM. To produce the fine powder used in the X-ray diffraction (XRD) measurements, some sample material was taken and crushed in an agate mortar to a grain size of approximately 1 µm to 10 µm ("X-ray fine"). The correct grain size was checked with a light microscope. Si-powder was used as internal standard to determine the zero shift of the X-ray diffractometer. The Rietveld analysis of the XRD patterns were done with the software FullProf Suite (Rodriguez-Carvajal, 2005). Kroll and Ribbe (1980) defined the degree of Al,Si order of plagioclase feldspars with the aluminum content of the $T_1 0$ site subtracted by the mean probability to find an aluminum ion in the $T_1 m$, the $T_2 0$ and the $T_2 m$ site $\left(t_1 0 - \langle t_1 m\rangle = t_1 0 - \frac{1}{3}\left(t_1 m + t_2 m + t_2 m\right)\right)$. The value of $t_1 0 - \langle t_1 m\rangle$ is calculated with the γ angle of the unit cell and on the An content.

2.2. Infrared analyses

For the IR measurements, all samples were crushed in a steel mortar and/or agate mortar and sieved to grain sizes up to 25 µm, 25 µm to 63 µm, 63 µm to 125 µm, 125 µm to 250 µm, and a remaining fraction of grains larger than 250 µm. The mid-infrared measurements were performed using a Bruker 70v FTIR spectrometer equipped with a grazing angle unit A513 and a liquid nitrogen cooled mercury cadmium telluride (MCT) detector at the Infrared and Raman for Interplanetary Spectroscopy (IRIS) lab at the Institut für Planetologie at the WWU. All spectra were acquired at pressures of 2 hPa and room temperature (ca. 23 °C to 25 °C.) As standard, we used the spectrum of a commercially available rough gold standard (INFRAGOLD™). We used powder samples to simulate regolith, which covers the surfaces of atmosphereless terrestrial bodies. The powder samples were placed in aluminum sample holder 1 cm in diameter and flattened with a spatula. Each grain size fraction was measured at two different geometries, with an incident angle of 20° and emergent angle of 30° (i20° e30°) and with incident and emergent angle of 13° (i13° e13°). Each single channel spectrum of sample and background were calculated through Fourier transformation of 512 single interferogram scans in double-sided forward-backward scan mode. The reflectance was calculated as the ratio of sample single spectrum to background single channel spectrum ($I_{sample}/I_{reference}$).

Mid-infrared spectra of silicate minerals are characterized by (1) the Christiansen feature (CF, ≈7.5 µm to 9 µm), which is a minimum in reflectance spectra caused by a rapid change of the refractive index by the region of the Reststrahlen Bands (RBs, ≈9 µm to 12 µm), which are related to stretching of Si-Si, Si(Al)-O, and Si-O bonds of the Si-O tetrahedrons, and (3) the Transparency Feature (TF, ≈11 µm to 13 µm) in spectra of grain sizes below ~70 µm, which is a broad peak and caused by stronger volume-scattering compared to surface-scattering (Pieters and Englert, 1993; Iiishi et al., 1971). A reduced sample grain size results in reduced reflectance values and broader RB peaks (Pieters and Englert, 1993).

Malcherek et al. (1995) proposed autocorrelation analysis of infrared absorption spectra to investigate the Al,Ge ordering in barium-germanium feldspars. The autocorrelation technique is sensitive to the width of the analyzed peaks in the spectra. Reitze et al. (2020) determined the degree of order as well as the Or content of alkali feldspars with the autocorrelation method. From there, we analyzed the feldspar infrared spectra not only in terms of band positions of CF but also with the autocorrelation method from 7.12 µm to 12.11 µm (825 cm^{-1} to 1376 cm^{-1}), which covers the region of the RBs. From the autocorrelation function we used the width ω of a Gaussian curve fit to the central peak from -26 cm^{-1} to 26 cm^{-1} of the autocorrelation function.

The infrared spectra produced in this study are obtainable from the IRIS database at www.uni-muenster.de/Planetology (Weber et al., 2018).

3. Results

3.1. Chemical composition and state of order

The results of the sample characterization are listed in Table 1. ID 125 albite is fully ordered ($t_1 0 - \langle t_1 m\rangle = 0.99$) and its chemical composition is Ab_{99}. The intermediate and high albite samples (ID 164, 165, 166, 167) are prepared through heating of the ID 125 sample and thus differ only in the degree of order (compare Reitze et al. (2020) for further information). The degree of order of ID 164 is 0.90, ID 165 is 0.52, ID 166 is 0.48, and ID 167 is 0.05. Sample ID 84 is an oligoclase with An_{12} and a degree of order of 0.75. ID 6 oligoclase (An_{19}) is more ordered ($t_1 0 - \langle t_1 m\rangle) = 0.63$) than ID 5 oligoclase ($An_{27}$) with $t_1 0 - \langle t_1 m\rangle = 0.49$. The analyzed andesine sample (ID 168, An_{39}) has $t_1 0 - \langle t_1 m\rangle = 0.24$. The synthetic An_{48} sample (ID 127) has $t_1 0 - \langle t_1 m\rangle = 0.14$. ID 2 labradorite ($An_{53}$) has a degree of Al,Si order of $t_1 0 - \langle t_1 m\rangle = 0.41$, whereas sample ID 28 labradorite (An_{51}) has $t_1 0 - \langle t_1 m\rangle = 0.37$. The labradorite sample ID 190 has an anorthite content of 0.66 and the degree of order is 0.16. As expected, the synthetic anorthite sample (An_{99}) has a very low degree of order of 0.02.

Fig. 1 shows the dependence of the degree of order depending on the γ angle of the unit cell and the An content for our samples calculated with the equation given by Kroll and Ribbe (1980).

3.2. FTIR spectra

Fig. 2 shows plagioclase mid-IR spectra for grain sizes between 63 µm and 125 µm and observation geometries with incident angles of 20 ° and emergent angles of 30 °. The CF shifts from approximately 7.73 µm (~1294 cm^{-1}) in the sodium endmember (mean) to 8.10 µm (1234 cm^{-1}) in anorthite (ID 126) (Table 1). The region of the RB is strongly affected by the chemical composition as well as the degree of Al,Si order. The spectrum of the low albite ID 125 shows four intense RBs and one large shoulder. The spectra of the more disordered sample ID 167 (equal to ID 164 165, and 166, compare Reitze et al. (2020)) do not show these strong bands due to the lower degree of Al,Si order but rather only two broad RBs. Spectra of the plagioclases with intermediate chemical compositions and lower degrees of order also show two strong RBs and larger shoulders only. Samples ID 2 and ID 190 show four strong

Table 1
Cation in wt%, lattice parameter in Å respectively degree, derived values of An-, Ab-, Or-content, and degree of order, as well as the wavenumber of the Christiansen feature. Uncertainty of the last digit in brackets.

ID/ Parameter	125 natural	163 natural treated	164 natural treated	165 natural treated	166 natural treated	167 natural treated	84 natural	6 natural	5 natural	168 natural	127 synthetic	28 natural	2 natural	190 natural	126 synthetic
Na	3.10	3.10	3.10	3.10	3.10	3.10	2.66	2.36	2.07	1.794	1.55	1.39	1.35	0.992	0.00
Mg	0.00	0.00	0.00	0.00	0.00	0.00	0.00	0.00	0.00	0.002	0.00	0.00	0.00	0.030	0.00
Al	3.01	3.00	3.00	3.00	3.00	3.00	3.39	3.48	3.72	4.220	4.48	4.45	4.42	4.938	6.01
Si	8.96	8.97	8.97	8.97	8.97	8.97	8.58	8.50	8.26	7.791	7.52	7.54	7.53	7.037	6.03
K	0.00	0.00	0.00	0.00	0.00	0.01	0.03	0.06	0.10	0.025	0.00	0.05	0.06	0.020	0.00
Ca	0.01	0.00	0.00	0.00	0.00	0.00	0.39	0.57	0.80	1.158	1.44	1.50	1.56	1.924	2.91
Fe	0.00	0.00	0.00	0.00	0.00	0.00	0.00	0.00	0.01	0.011	0.004	0.01	0.03	0.046	0.00
Ti	0.00	0.00	0.00	0.00	0.00	0.00	0.00	0.00	0.00	0.002	0.00	0.00	0.00	0.005	0.00
Cr	0.00	0.00	0.00	0.00	0.00	0.00	0.00	0.00	0.00	0.001	0.00	0.00	0.00	0.001	0.00
Mn	0.00	0.00	0.00	0.00	0.00	0.00	0.00	0.00	0.00	0.002	0.00	0.00	0.00	0.003	0.00
Ab	100	100	100	100	100	100	86	79	70	60	52	47	45	34	0
An	0	0	0	0	0	0	13	19	27	39	48	51	53	66	100
Or	0	0	0	0	0	0	1	2	3	1	0	2	2	1	0
a	8.132(2)	8.146(3)	8.144(5)	8.142(3)	8.137(3)	8.158(2)	8.151(1)	8.1540(8)	8.166(1)	8.157(2)	8.155(2)	8.1720(7)	8.1761(9)	8.171(3)	8.180(4)
b	12.783(2)	12.799(4)	12.816(8)	12.846(6)	12.826(6)	12.874(3)	12.813(2)	12.827(1)	12.849(2)	12.864(1)	12.870(2)	12.859(1)	12.860(1)	12.872(3)	12.872(2)
c	7.159(2)	7.144(2)	7.149(2)	7.126(3)	7.130(2)	7.111(1)	7.142(1)	7.1328(5)	7.1244(8)	7.1103(9)	7.103(1)	7.1105(5)	7.1114(6)	7.101(2)	14.1727(9)
α	94.29(2)	94.22(3)	94.21(5)	93.92(5)	94.02(4)	93.51(2)	94.01(2)	93.94(1)	93.73(2)	93.52(2)	93.48(2)	93.568(1)	93.59(1)	93.49(3)	93.14(2)
β	116.59(2)	116.57(2)	116.61(3)	116.47(4)	116.47(2)	116.45(2)	116.52(1)	116.470(7)	116.40(1)	116.25(1)	116.08(1)	116.260(6)	116.251(8)	116.08(2)	115.84(1)
γ	87.69(2)	88.07(3)	87.93(5)	89.33(5)	89.08(4)	90.22(2)	88.51(2)	88.876(9)	89.31(2)	90.10(2)	90.37(2)	89.785(8)	89.69(1)	90.51(3)	91.25(4)
V	663.6(2)	664.4(3)	665.3(6)	665.5(5)	664.4(4)	667.0(3)	665.8(2)	666.1(1)	668.0(2)	667.6(2)	667.9(2)	668.50(9)	669.1(1)	669.1(3)	1339.3(3)
$t_1 0 - \langle t_1 m \rangle$	0.99(19)	0.85(15)	0.90(16)	0.54(15)	0.48(10)	0.06(8)	0.75(12)	0.63(10)	0.49(8)	0.20(6)	0.13(5)	0.37(8)	0.42(8)	0.15(8)	0.02(16)
CF µm	1296	1294	1292	1298	1296	1291	1291	1292	1274	1266	1261	1264	1259	1251	1234

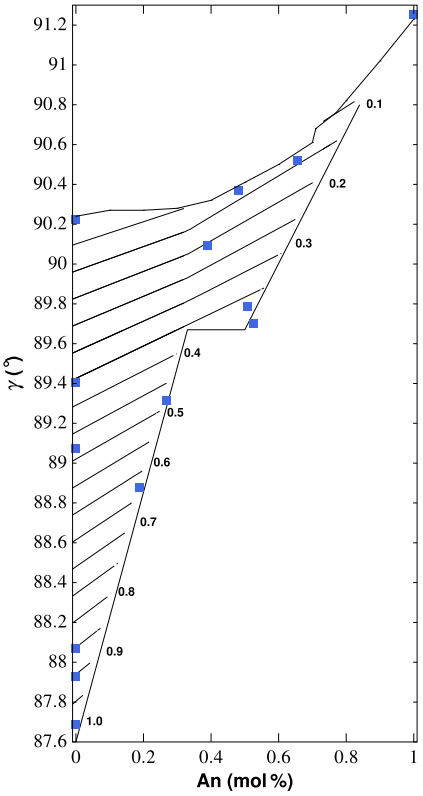

Fig. 1. The γ angle of the unit cell determined from powder XRD Rietveld refinements depending on the An content of our samples (blue squares). The plot is contoured in 0.05 steps from 0.1 to 1 for the possible degree of the Al,Si order ($t_1 0 - \langle t_1 m \rangle = t_1 0 - \frac{1}{3}(t_1 m + t_2 m + t_2 m)$) of the plagioclase series (see Kroll and Ribbe, 1980, for details). (For interpretation of the colors in the figure(s), the reader is referred to the web version of this article.)

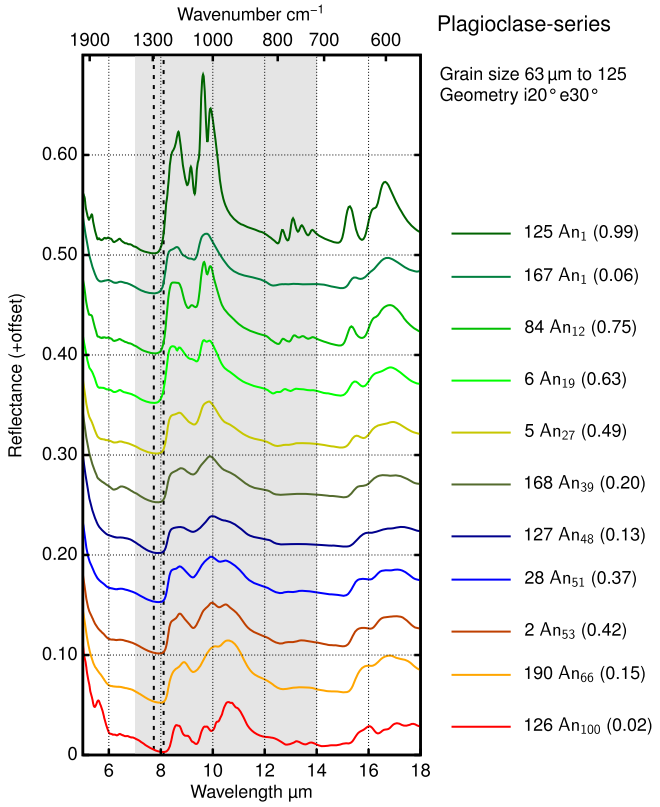

Fig. 2. Reflectance spectra of individual plagioclase samples with grain sizes between 63 µm to 125 µm and incident angles of 20 ° and emergent angles of 30 ° with different chemical compositions (except for ID 125 and ID 167) from top An_1 to bottom An_{99} and degrees of Al,Si order in brackets. The gray region indicates the measurement range of MERTIS from 7 µm to 14 µm (1429 cm^{-1} to 714 cm^{-1}); the two dotted lines indicate the An content-depended shift of the CF from ID 125 (low) albite (top, 7.73 µm,1294 cm^{-1}) to anorthite (bottom, 8.11 µm,1233 cm^{-1}). The spectral contrast of the RBs decreases due to increasing An contents and decreasing degrees of order. Spectra of samples with ID 164, ID 165, and 166 are not shown, see Reitze et al. (2020) for the spectra.

RBs, but compared with the ID 125 spectrum, broader RBs. The spectrum of the anorthite sample (ID 126) shows two broad RBs and one with less intensity. Between 12 µm and 14 µm (833 cm^{-1} and 714 cm^{-1}), only low albite shows four clear bands and anorthite two bands; all other spectra are smooth in this region. The wavelengths of the RBs shift with chemical compositions from albite to anorthite to longer wavelengths.

The spectra of the smallest grain sizes are reduced in spectral contrast, so that the RBs are not as well-resolved as in the spectra of the larger grain sizes (Fig. 3). In contrast to the spectra of the larger grain sizes, the small grain size spectra show a strong TF between 10.5 µm and13 µm (952 cm^{-1} and 769 cm^{-1}). It splits into one larger peak around 12 µm (833 cm^{-1}) and a large shoulder around 11 µm (909 cm^{-1}) with increasing An content. In addition, both, the peak and the shoulder, shift towards longer wavelengths with increasing An contents to a peak wavelength of 12.33 µm (811 cm^{-1}) for An_{99}. In the spectra of the samples with intermediate compositions (ID 28, 127, and 168), the TFs are very different from each other. In the ID 127 spectrum, there is only a peak visible at 12.17 µm (822 cm^{-1}) and no shoulder. The ID 28 spectrum is characterized by a peak at 12.05 µm (830 cm^{-1}) and a stronger shoulder at around 11.51 µm (869 cm^{-1}). In contrast, in the ID 168 spectrum, the peak is at 12.11 µm (826 cm^{-1}) and a weak shoulder is visible at around 11.53 µm (867 cm^{-1}).

4. Discussion

4.1. General remarks

The CF is visible in spectra of samples with larger and smaller grain sizes, does not disappear in experimentally shocked plagioclase spectra (Nash and Salisbury, 1991; Johnson, 2012), and can be used for analyses of remote sensing data. The CF of different plagioclase samples shifts towards high wavelength due to shock effects (Johnson, 2012). In contrast, peak fitting in reflectance infrared spectra is a difficult task because of broad overlapping RB peaks and their disappearance in spectra of samples with small grain sizes. Thus, we used the autocorrelation method to analyze the spectra of unshocked plagioclase and correlated the wavelength of the CF with data gathered from the autocorrelation method in order to avoid peak fitting of RBs.

4.2. Christiansen feature analyses

Conel (1970) provided a function to determine the SiO_2 content of thin films of plagioclase glass samples from the wavenumber of the CF and Nash and Salisbury (1991) showed that the wavelength of the CF in plagioclase spectra is unaffected by the degree of vitrification at least for samples that were neither shocked nor space weathered (compare section 4.5). We compared the CF of our samples with their SiO_2 contents (Fig. 4). CF and SiO_2 contents of our samples and the samples of Nash and Salisbury (1991) do not match the curves given by Conel (1970). This is probably due to the observation geometry and the general shape of the spectra around the CF (Pieters and Englert, 1993). The reflectance trough around the CF is relatively broad, and noise makes the exact determination of the lowest intensity difficult. Therefore, the smallest reflectance value is not necessarily the CF or shifted to another

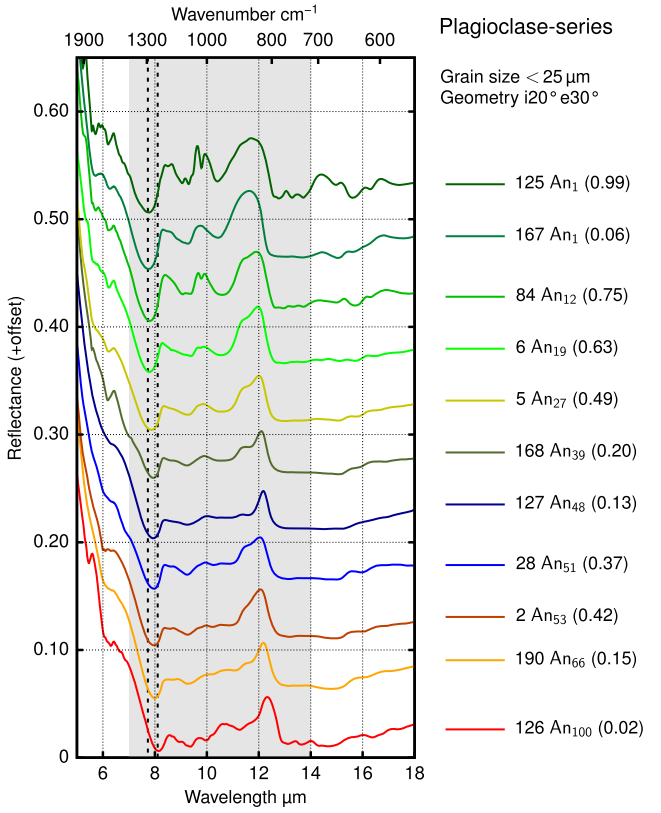

Fig. 3. Reflectance spectra of individual plagioclase samples with grain sizes smaller than 25 µm and incident angles of 20 ° and emergent angles of 30 ° with different chemical compositions (except for ID 125 and ID 167) from top An_1 to bottom An_{99} and degrees of Al,Si order in brackets. The gray region indicates the measurement range of MERTIS from 7 µm to 14 µm (1429 cm^{-1} to 714 cm^{-1}); the two dotted lines indicate the An content-depended shift of the CF from ID 125 (low) albite (top, 7.73 µm,1294 cm^{-1}) to anorthite (bottom, 8.11 µm,1233 cm^{-1}). The spectral contrast of the RBs decreases due to increasing An contents and decreasing degrees of order. Spectra of samples with ID 164, ID 165, and 166 are not shown, see Reitze et al. (2020) for the spectra. The TFs around 12 µm become shallower with increasing An contents.

wavelength. However, our data confirm, that the wavelength of the CF is due to the An-content of the plagioclase samples.

4.3. Autocorrelation analysis of RBs in combination with Christiansen feature analyses

Atkinson et al. (1999) used the autocorrelation technique to analyze the degree of order in absorption spectra of plagioclases, and did not detect dependencies in the wavelength region between 7.14 µm and 12.05 µm (1400 cm^{-1} and 830 cm^{-1}). However, a composition-dependence was identified. In contrast, reflectance spectra of low albite sample ID 125 and the high albite sample ID 167, which both have the same chemical compositions, show that the region of the RBs is affected by the degree of order (e.g., Fig. 2). Reflectance spectra of intermediate plagioclases show a similar behavior, i.e., broadening and disappearance of peaks (e.g., Spectra ID 167 and ID 5 in Fig. 2). Thus, the wavelength region of the plagioclase RBs is affected by both, chemical composition as well as degree of Al,Si order. To distinguish among these two overlapping effects, we used the wavelength of the CF to have a parameter which only depends on the chemical composition (e.g., Conel, 1970; Nash and Salisbury, 1991).

As described above, the grain size distribution also affects the shape of the RBs. The hermean regolith is thought to be similar to lunar mature anorthite regolith at least to first order (Blewett et al., 2002). Analyses of samples of the Apollo 17 landing site showed different grain size distributions caused by different soil maturities (McKay et al., 1974). This makes analyses of different grain size fractions necessary to provide spectra which best represent the regolith.

Table 2
Results for fit parameters depending on the grain size fraction.

Parameter	< 25 µm	25 µm to 63 µm	63 µm to 125 µm
a_1 cm^{-1}	-0.1124	0.0322	0.1072
a_2 cm^{-1}	-4.9989	0.9458	2.8365
a_3 cm^{-2}	0.0048	-0.0005	-0.0021
a_4 *dimensionless*	128.2270	-44.9624	-139.3040
a_5 cm^{-2}	-0.0220	-0.0036	-0.0014

Fig. 5 shows the dependence of the CF wavelength and ω fitted to the degree of order (from the XRD measurements) for the grain size fraction from 63 µm to 125 µm. The fit function has the form of $f(x) = a_1 \cdot \nu + a_2 \cdot \omega + a_3 \cdot \nu \cdot \omega + a_4 + a_5 \cdot \omega^2$, representing a plane in a three-dimensional space. The same fit function was applied to values derived from spectra of samples with grain sizes of 25 µm to 63 µm and grain sizes smaller than 25 µm (See Table 2 for the calculated values).

Fig. 6 shows the deviation of the plane fit taken from Fig. 5. The comparison between the XRD and the infrared reflectance-derived degree of order shows that for 10 samples (ID 125, 163, 165, 166, 127, 190, 2, 5, 28, and 84) the degree of order calculated with the later method lies within the range of uncertainty of the powder XRD-derived degree of order. The mean deviation of the degree of order between the two methods for the 10 samples is 0.06. For the other 5 samples (ID 164, 167, 126, 168, and 6) the mean deviation is larger (0.22). Comparing all samples in this grain size range, the mean deviation is 0.11. These values imply, that the degree of order of samples with grain sizes between 63 µm and 125 µm can be determined with a mean error of around 0.11 using FTIR data. Fig. 7 shows the deviation between the degree of order calculated with XRD and based on the infrared spectra for grain sizes between 25 µm and 63 µm. For these grain size range the mean deviation of all samples is 0.13. For grain sizes smaller than 25 µm (Fig. 8), the mean deviation of the determined degree of order is 0.10.

The differences of the fit functions between the different grain sizes indicates that knowledge of the grain size distributions of analyzed surfaces is desirable for accurate results. In the case of Mercury grain size distributions may be derived from MERTIS thermal inertia data taking into account the mean density of the regolith (Bauch et al., 2014) related to the mean grain size. In addition, the intensity of the TF compared to the RBs can give hints on the grain size distribution.

4.4. Transparency feature description

We describe the behavior of the TF in the spectra of the small grain sizes, because the surfaces of atmosphereless bodies are highly affected by micrometeorite bombardment, which causes the formation of fine-grained regoliths. For example, the Moon's mature regolith grain size distribution has a large maximum at around 62 µm (McKay et al., 1974). Moreover, the TF is coupled with the chemical composition of minerals and rocks (e.g., Salisbury and Walter, 1989). The observed shift and peak splitting of the TF described above could be explained by the degree of Al,Si order. The shoulder becomes weaker, if the degree of order is reduced, but there is also a chemical composition effect, which overlaps with the effect of Al,Si ordering. Our labradoritic samples ID 127, ID 28, and ID 2 are relatively similar in their chemical composition but differ in the degree of Al,Si order. Hence, the strongest TF peak is about at the same wavelength for those three samples, although the intensity of the shoulder part of the TF differs

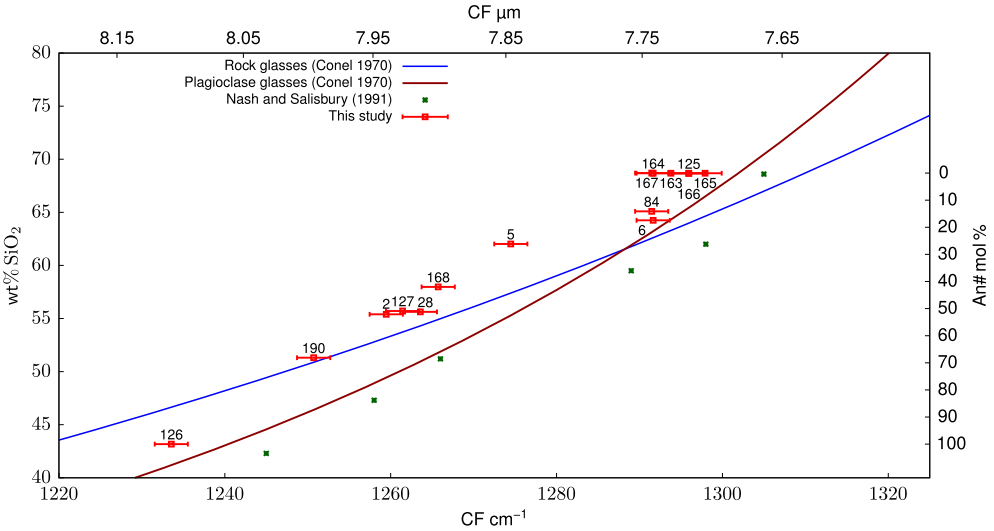

Fig. 4. Wavenumber/wavelength of the Christiansen feature compared with the SiO_2/An contents of our samples and values taken by Nash and Salisbury (1991). The trends given by Conel (1970) are not matched neither by our samples nor by the samples measured by Nash and Salisbury (1991). The mean of the standard deviation of the SiO_2 is less than 0.5. The CF of our samples is taken from spectra measured at i20/e30, except for sample ID 84 where we used the i13/e13 geometry because of noisy spectrum.

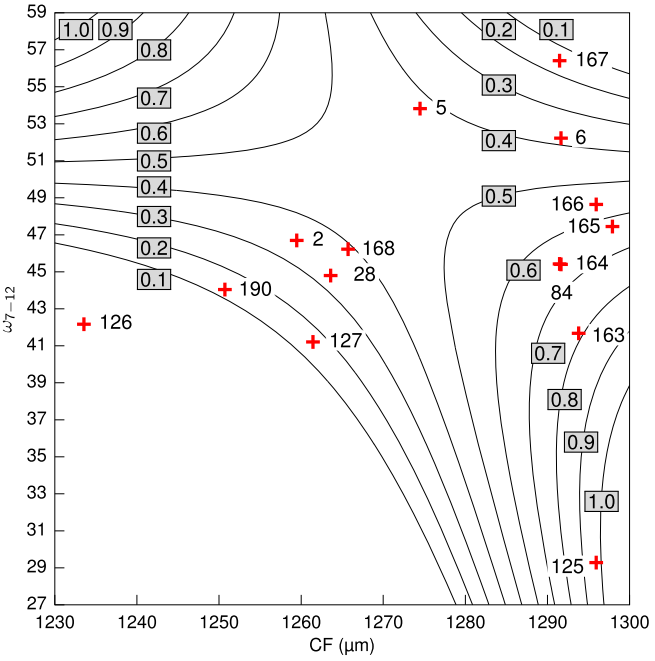

Fig. 5. Position of the CF compared to the ω value for the grain size from 63 µm to 125 µm. The plot is contoured in 0.1 steps for the plane fit to the degree of order.

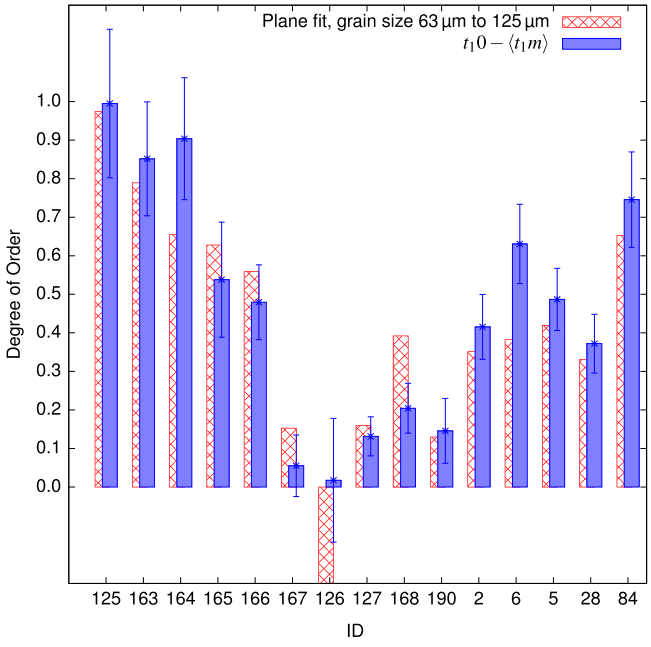

Fig. 6. Comparison between the degree of order determined on the basis of XRD data and the plane fit using the ω value and CF wavenumber for all samples of this study with grain sizes between 63 µm and 125 µm. For ten of the 15 samples the degree of order determined with CF and ω (red shaded boxes) is within the range of uncertainty of the XRD derived values (blue boxes with errorbar).

strongly. In the more ordered samples ID 28 and ID 2, the shoulder is clearly identifiable in contrast to the more disordered sample ID 2. This effect is especially important for the interpretation of MERTIS observations, because Mercury's surface is thought to be rich in labradorite (Sprague et al., 1997).

4.5. Implications for space weathering, shock effects, and maturity of the regolith

Micrometeorite bombardment reduces the spectral contrast in the RB region of plagioclases with an andesinic to labradoritic composition (Moroz et al., 2014). In addition, Moroz et al. (2014) observed the rise of the TF in spectra of space weathered analog material. Moroz et al. (2014) argued that these observed changes in their spectra are due to a change in the porosities and grain sizes of their samples. Simulated micrometeorite bombardment by Weber et al. (2019) of pressed powder samples of olivine, pyroxene, and mixtures of both, showed a decrease of the TF correlated with agglutination of the surface. Moreover, analyses of lunar soils also show a shift of the CF due to space weathering (Lucey et al., 2017). Shock recovery experiments by Johnson (2012) and Johnson et al. (2003) showed a degradation of the RBs of plagioclase spectra and a decrease of the TF in their powder samples. At this point it is important to note that the degree of order is different to glass formation. The degree of Al,Si order is applied to complete crystalline material. Although, Johnson (2012) and Johnson et al. (2003) did not analyze the degree of order of the plagioclase samples, the spectra presented in both studies are thought to be

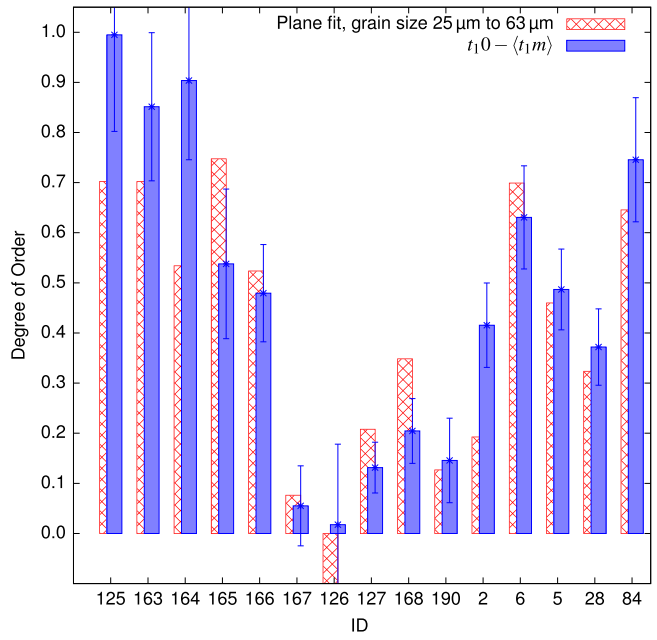

Fig. 7. Comparison between the degree of order determined on the basis of XRD data and the plane fit using the ω value and CF wavenumber for all samples of this study with grain sizes between 25 µm and 63 µm. For eight of the 15 samples the degree of order determined with CF and ω (red shaded boxes) is within the range of uncertainty of the XRD derived values (blue boxes with errorbar).

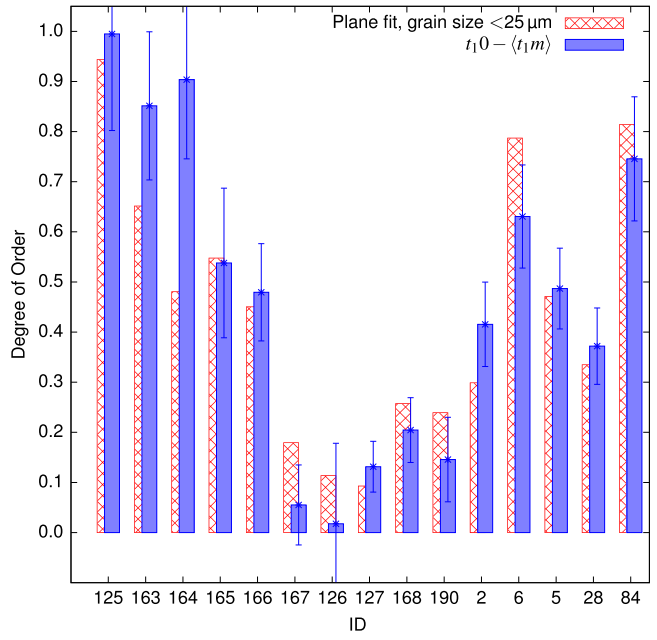

Fig. 8. Comparison between the degree of order determined on the basis of XRD data and the plane fit using the ω value and CF wavenumber for all samples of this study with grain sizes smaller 25 µm. For ten of the 15 samples the degree of order determined with CF and ω (red shaded boxes) is within the range of uncertainty of the XRD derived values (blue boxes with errorbar).

influenced by the formation of diaplectic glass due to the shock. Especially spectra of higher shocked albite-rich rocks in Johnson et al. (2003) can be confused with spectra of albites with lower degree of Al,Si order. This highlights the necessity of detailed analog sample characterization prior to analyses of remote sensing data. In addition, both processes (micrometeorite bombardment and shock) may confound with spectra of more disordered samples with larger grain sizes. The observed rapid change of the Al,Si order of experimentally shocked plagioclases after heating by Ostertag and Stöffler (1982) may also affect the infrared spectra. In fact, in the extensive study of Ostertag (1983) *only* single events were analyzed and the effect of residual temperature were tried to rule out through quenching of the samples after the shock event. The surfaces of planetary bodies without atmosphere are exposed to space weathering and impacts for millions to billions of years. In addition, large impacts will cause the formation of impact melts which serve as heat reservoir (Bischoff and Stöffler, 1984). Within these melts, high plagioclase feldspars will crystallize, cool down at a lower rate than at the surface, and preserve a specific degree of order. Reworking these impact melts by later impacts will transport this *fresher* material to the surface. The observed CF shift may be misinterpreted in terms of the chemical compositions of feldspar-bearing rocks. Hence, all spectral deconvolution procedures must consider (plagioclase) feldspars with different degrees of order in addition to space weathering effects.

5. Conclusions

We investigated mid-infrared spectra of well-characterized plagioclase samples with different states of Al,Si order in the wavelength region between 7 µm and 14 µm (1429 cm^{-1} and 714 cm^{-1}). The spectra show clear changes not only due to the chemical composition of the samples but also due to the degree of Al,Si order. Hence we combined the position of the CF with ω, which is the width of a fit to the central part of the autocorrelation function of the spectral range between 7.12 µm and 12.11 µm (1405 cm^{-1} and 826 cm^{-1}) and fitted these data to the degree of Al,Si order derived from XRD measurements to derive a function which give the degree of order depending on the CF and ω. The degree of order of a sample could be determined within a mean uncertainty of approximately ± 0.11, by comparing the fitted functions with XRD derived values, applied to different grain size fractions spectra This result is important for deconvolution of data returned by MERTIS as well as other future space missions as (1) it shows that the degree of Al,Si order of plagioclases cannot be neglected in laboratory analog studies and proves the need for accurate sample characterization of the laboratory analog materials; (2) the information about the degree of order can give hints about the formation history of the surfaces; (3) the identification of the Al,Si order related spectral changes are necessary to distinguish these order related effects from chemical composition effects.

In addition, it is shown that the degree of order affects the spectral shape of the TF within the smallest analyzed grain size fraction, i.e., smaller than 25 µm. Spectra of samples with a chemical composition around An_{51} and with differing degrees of Al,Si order show distinct different TFs. This is an additional way to determine the degree of order of the plagioclases on the surface and can help to identify the surface mineralogy, because Mercury's surface is thought to be labradoritic at least in some regions (e.g., Sprague et al., 1997). The results of this study help to improve the deconvolution of data returned by MERTIS as well as other future space missions because it extends the available spectral database of well-characterized minerals.

CRediT authorship contribution statement

Maximilian P. Reitze: Conceptualization, Methology, Investigation, Writing – Original Draft. **Iris Weber:** Investigation, Conceptualization, Writing – Review & Editing. **Andreas Morlok:** Methology, Writing – Review & Editing. **Aleksandra N. Stojic:** Writing – Review & Editing. **Karin E. Bauch:** Visualization. **Harald Hiesinger:** Resources, Writing – Review & Editing, Funding acquisition. **Jörn Helbert:** Supervision.

Declaration of competing interest

The authors declare that they have no known competing financial interests or personal relationships that could have appeared to influence the work reported in this paper.

Acknowledgements

Many thanks to Herbert Kroll for the supply of samples ID 125, 126, and 127 and for his time for detailed discussions, Stephan Klemme, Christian Renggli for their help and permission to use their laboratory, Ludger Buxtrup for technical support with the ovens, Peter Schmid-Beuermann for help with XRD, and Uta Rodehorst for advice and the possibility of using the laboratory at the MEET. This work is partly supported by the DLR funding 50 QW 1701 in the framework of the Bepi-Colombo mission.

References

Atkinson, A.J., Carpenter, M.A., Salje, E.K.H., 1999. Hard mode infrared spectroscopy of plagioclase feldspars. Eur. J. Mineral. 11, 7–21.

Bauch, K.E., Hiesinger, H., Helbert, J., Robinson, M.S., Scholten, F., 2014. Estimation of lunar surface temperatures and thermophysical properties: test of a thermal model in preparation of the MERTIS experiment onboard BepiColombo. Planet. Space Sci. 101, 27–36. https://doi.org/10.1016/j.pss.2014.06.004.

Bennett, C.J., Pirim, C., Orlando, T.M., 2013. Space-weathering of solar system bodies: a laboratory perspective. Chem. Rev. 113, 9086–9150. https://doi.org/10.1021/cr400153k.

Bischoff, A., Stöffler, D., 1984. Chemical and structural changes induced by thermal annealing of shocked feldspar inclusions in impact melt rocks from Lappajarvi crater, Finland. Proc. Lunar Planet. Sci. Conf. 89, B645–B656. https://doi.org/10.1029/JB089iS02p0B645.

Blewett, D.T., Hawke, B.R., Lucey, P.G., 2002. Lunar pure anorthosite as a spectral analog for Mercury. Meteorit. Planet. Sci. 37, 1245–1254. https://doi.org/10.1111/j.1945-5100.2002.tb00893.x.

Cintala, M.J., 1992. Impact-induced thermal effects in the lunar and mercurian regoliths. J. Geophys. Res., Planets 97, 947–973. https://doi.org/10.1029/91JE02207.

Conel, J., 1970. A new method for determining SiO_2 abundance in silicate glass from powder film transmission measurements. In: Space Programs Summary, Vol. III. Supporting Research and Advanced Development. Jet Propulsion Laboratory, pp. 37–63.

Evans, L.G., Peplowski, P.N., Rhodes, E.A., Lawrence, D.J., McCoy, T.J., Nittler, L.R., Solomon, S.C., Sprague, A.L., Stockstill-Cahill, K.R., Starr, R.D., Weider, S.Z., Boynton, W.V., Hamara, D.K., Goldsten, J.O., 2012. Major-element abundances on the surface of Mercury: results from the MESSENGER Gamma-Ray spectrometer. J. Geophys. Res., Planets 117, E00L07. https://doi.org/10.1029/2012JE004178.

Hafner, S., Laves, F., 1957. Ordnung/Unordnung und Ultrarotabsorption II. Variation der Lage und Intensitäten. Zur Struktur von Orthoklas und Adular. Z. Kristallogr. 109, 204–225. https://doi.org/10.1524/zkri.1957.109.1-6.204.

Harmon, J.K., Slade, M.A., Rice, M.S., 2011. Radar imagery of Mercury's putative polar ice: 1999–2005 Arecibo results. Icarus 211, 37–50.

Hecker, C., van der Mijde, M., van der Meer, F.D., 2010. Thermal infrared spectroscopy on feldspars - successes, limitations and their implications for remote sensing. Earth-Sci. Rev. 103, 60–70.

Hiesinger, H., Helbert, J., MERTIS Co-I Team, 2010. The Mercury Radiometer and Thermal Infrared Spectrometer (MERTIS) for the BepiColombo mission. Planet. Space Sci. 58, 144–165.

Hiesinger, H., Helbert, J., Alemanno, G., Bauch, K.E., D'Amore, M., Maturilli, A., Morlok, A., Reitze, M.P., Stangarone, C., Stojic, A.N., Varatharajan, I., Weber, I., MERTIS Co-I Team, 2020. Studying the composition and mineralogy of the hermean surface with the Mercury Radiometer and Thermal Infrared Spectrometer (MERTIS) for the BepiColombo mission: an update. Space Sci. Rev. 216 (6), 110.

Iiishi, K., Tomisaka, T., Kato, T., Umegaki, Y., 1971. Isomorphous substitution and infrared and far infrared spectra of the feldspar group. Neues Jahrb. Mineral. Abh. 115, 98–119.

Johnson, J., Horz, F., Staid, M., 2003. Thermal infrared spectroscopy and modeling of experimentally shocked plagioclase feldspars. Am. Mineral. 88, 1575–1582.

Johnson, J.R., 2012. Thermal infrared spectra of experimentally shocked andesine anorthosite. Icarus 221, 359–364.

Kroll, H., Ribbe, P.H., 1980. Determinative diagrams for Al, Si order in plagioclases. Am. Mineral. 65, 449–457.

Laves, F., Hafner, S., 1956. Ordnung/Unordnung und Ultrarotabsorption I. (Al, Si)-Verteilung in Feldspäten. Z. Kristallogr. 108, 52–63. https://doi.org/10.1524/zkri.1956.108.1-2.52.

Loewenstein, W., 1954. The distribution of aluminum in the tetrahedra of silicates and aluminates. Am. Mineral. 39, 92–96.

Lucey, P.G., Greenhagen, B.T., Song, E., Arnold, J.A., Lemelin, M., Hanna, K.D., Bowles, N.E., Glotch, T.D., Paige, D.A., 2017. Space weathering effects in Diviner Lunar Radiometer multispectral infrared measurements of the lunar Christiansen feature: characteristics and mitigation. Icarus 283, 343–351. https://doi.org/10.1016/j.icarus.2016.05.010.

Lyon, R., 1964. Evaluation of infrared spectrometry for compositional analysis of lunar and planetary soils part II: rough and powdered surfaces. NASA Rept. CR-100.

Malcherek, T., Kroll, H., Schleiter, M., Salje, E.K.H., 1995. The kinetics of the monoclinic to monoclinic phase transition in $BaAl_2Ge_2O_8$-feldspar. Phase Transit. 55, 199–215.

McKay, D.S., Fruland, R.M., Heiken, G.H., 1974. Grain size and the evolution of lunar soils. In: Lunar and Planetary Science Conference Proceedings, vol. 1, pp. 887–906.

Morlok, A., Klemme, S., Weber, I., Stojic, A., Sohn, M., Hiesinger, H., 2017. IR spectroscopy of synthetic glasses with Mercury surface composition: analogs for remote sensing. Icarus 296, 123–138. https://doi.org/10.1016/j.icarus.2017.05.024.

Morlok, A., Klemme, S., Weber, I., Stojic, A., Sohn, M., Hiesinger, H., Helbert, J., 2019. Mid-infrared spectroscopy of planetary analogs: a database for planetary remote sensing. Icarus 324, 86–103. https://doi.org/10.1016/j.icarus.2019.02.010.

Morlok, A., Hamann, C., Martin, D., Weber, I., Joy, K.H., Hiesinger, H., Wogelius, R., Stojic, A.N., Helbert, J., 2020. Mid-infrared spectroscopy of laser-produced basalt melts for remote sensing application. Icarus 335, 113410. https://doi.org/10.1016/j.icarus.2019.113410.

Moroz, L.V., Starukhina, L.V., Rout, S.S., Sasaki, S., Helbert, J., Baither, D., Bischoff, A., Hiesinger, H., 2014. Space weathering of silicate regoliths with various FeO contents: new insights from laser irradiation experiments and theoretical spectral simulations. Icarus 235, 187–206.

Murray, B.C., 1975. Mercury. Sci. Am. 233, 58–69.

Nash, D.B., Salisbury, J.W., 1991. Infrared reflectance spectra (2.2-15μm) of plagioclase feldspars. Geophys. Res. Lett. 18, 1151–1154.

Nittler, L.R., Starr, R.D., Weider, S.Z., McCoy, T.J., Boynton, W.V., Ebel, D.S., Ernst, C.M., Evans, L.G., Goldsten, J.O., Hamara, D.K., Lawrence, D.J., McNutt Jr., R.L., Schlemm II, C.E., Solomon, S.C., Sprague, A.L., 2011. The major-element composition of Mercury's surface from MESSENGER X-ray spectrometry. Science 333, 1847–1850.

Ostertag, R., 1983. Shock experiments on feldspar crystals. In: Lunar and Planetary Science Conference Proceedings, vol. 88, pp. B364–B376.

Ostertag, R., Stöffler, D., 1982. Thermal annealing of experimentally shocked feldspar crystals. In: Lunar and Planetary Science Conference Proceedings, vol. 87, pp. A457–A464.

Pieters, C.M., Englert, P.A.J. (Eds.), 1993. Topics in Remote Sensing 4. Remote Geochemical Analysis: Elemental and Mineralogical Composition. Cambridge University Press.

Reitze, M., Weber, I., Kroll, H., Morlok, A., Hiesinger, H., Helbert, J., 2020. Mid-infrared spectroscopy of alkali feldspar samples for space application. Mineral. Petrol. 114, 453–463.

Ribbe, P.H., 1983. Feldspar Mineralogy. De Gruyter, Berlin, Boston.

Rodriguez-Carvajal, J., 2005. Full Prof Suite. Lab. Brillouin (CEA-CNRS) CEA/Saclay, France.

Salisbury, J.W., Walter, L.S., 1989. Thermal infrared (2.5-13.5 μm) spectroscopic remote sensing of igneous rock types on particulate planetary surfaces. J. Geophys. Res., Solid Earth 94.

Scambos, T.A., Smyth, J.R., McCormick, T.C., 1987. Crystal-structure refinement of high sanidine from the upper mantle. Am. Mineral. 72, 973–978.

Solomon, S.C., Nittler, L.R., Anderson, B.J. (Eds.), 2018. Mercury: The View After MESSENGER. Cambridge University Press.

Sprague, A.L., Hunten, D.M., Lodders, K., 1995. Sulfur at Mercury, elemental at the poles and sulfides in the regolith. Icarus 118, 211–215.

Sprague, A.L., Nash, D.B., Witteborn, F., Cruikshank, D.P., 1997. Mercury's feldspar connection - Mid-IR measurements suggest plagioclase. Adv. Space Res. 19, 1507.

Sprague, A.L., Donaldson Hanna, K.L., Kozlowski, R.W.H., Helbert, J., Maturilli, A., Warell, J.B., Hora, J.L., 2009. Spectral emissivity measurements of Mercury's surface indicate Mg- and Ca-rich mineralogy, K-spar, Na-rich plagioclase, rutile, with possible perovskite, and garnet. Planet. Space Sci. 57, 364–383.

Vander Kaaden, K.E., McCubbin, F.M., Nittler, L.R., Peplowski, P.N., Weider, S.Z., Frank, E.A., McCoy, T.J., 2017. Geochemistry, mineralogy, and petrology of boninitic and komatitic rocks on the mercurian surface: insights into the mercurian mantle. Icarus 285, 155–168.

Varatharajan, I., Maturilli, A., Helbert, J., Alemanno, G., Hiesinger, H., 2019. Spectral behavior of sulfides in simulated daytime surface conditions of Mercury: supporting past (MESSENGER) and future missions (BepiColombo). Earth Planet. Sci. Lett. 520, 127–140. https://doi.org/10.1016/j.epsl.2019.05.020.

Vilas, F., Chapman, C.R., Matthews, M.S. (Eds.), 1988. Mercury. University of Arizona.

Weber, I., Morlok, A., Grund, T., Bauch, K.E., Hiesinger, H., Stojic, A., Grumpe, A., Wöhler, C., Klemme, S., Sohn, M., Martin, D.J.P., Joy, K.H., 2018. A mid-infrared reflectance database in preparation for space missions. In: LPSC, vol. 1430.

Weber, I., Morlok, A., Heeger, M., Adolphs, T., Reitze, M.P., Hiesinger, H., Bauch, K.E., Stojic, A.N., Arlinghaus, H.F., Helbert, J., 2019. Excimer laser experiments

on mixed silicates simulating space weathering on Mercury. In: EPSC-DPS Joint Meeting 2019, vol. 2019, EPSC-DPS2019-1325.

Weber, I., Stojic, A.N., Morlok, A., Reitze, M.P., Markus, K., Hiesinger, H., Pavlov, S.G., Wirth, R., Schreiber, A., Sohn, M., Hübers, H.-W., Helbert, J., 2020. Space weathering by simulated micrometeorite bombardment on natural olivine and pyroxene: a coordinated IR and TEM study. Earth Planet. Sci. Lett. 530, 115884. https://doi.org/10.1016/j.epsl.2019.115884.